Systematic study of ferroelectric, interfacial, oxidative, and doping effects on conductance of $Pt/BaTiO_3/Pt$ ferroelectic tunnel junctions

Lei Shen (沈雷),[1,*] Tiejun Zhou,[1] Zhaoqiang Bai,[2,1] Minggang Zeng,[2] Jing Qiang Goh,[2] Zhi-min Yuan,[1] Guchang Han,[1] Bo Liu,[1] and Yuan Ping Feng[2,†]

[1]*Data Storage Institute, Agency for Science Technology and Research, 5 Engineering Drive 1, Singapore 117608, Singapore*

[2]*Department of Physics, 2 Science Drive 3, National University of Singapore, Singapore 117542, Singapore*

(Received 1 November 2011; revised manuscript received 10 January 2012; published 9 February 2012)

Using the nonequilibrium Green's function method combined with density functional theory, we systematically study the ferroelectric, interfacial, oxidative, and doping effects on electron transport of $BaTiO_3$-based ferroelectric tunnel junctions ($Pt/BaTiO_3/Pt$). The ferroelectric effect reduces the tunneling conductance compared to nonferroelectric $BaTiO_3$ due to the large decay rate of the $\Delta 5$ (p_y and d_{yz}) band. The TiO_2-terminated interface shows a better tunneling conductance than the BaO-terminated interface since electrons mainly transport through the Ti_{3d}-O_p bonding state. Interfacial oxidation strongly reduces the conductance due to trapping of electrons and interfacial charge localization by additional O ions, while Nb doping enhances the conductance due to the delocalized distribution of charges on orbitals of the transport channel. Our studies provide a useful guide to practical applications of tunnel junctions with ferroelectric barriers.

DOI: 10.1103/PhysRevB.85.064105 PACS number(s): 73.40.Gk, 77.80.−e, 73.40.Rw, 71.15.Mb

I. INTRODUCTION

Rapid advances in data storage technology rely on high speed and large capacity nonvolatile memories. Currently a big issue (scaling) to conventional memories is expected to come up against physical and technical limits in the near future. To overcome this problem, functionalization by introducing new materials has been proposed as a new alternative to the conventional scaling technology. Candidates for equivalent scaling based on new materials, including resistance random access memories (RRAMs),[1,2] which uses a resistive switching phenomenon found in metal oxides and magnetoresistive random access memories (MRAMs),[3,4] which uses magnetic tunnel junctions. Recently, a new candidate has emerged: ferroelectric random access memories (FERAMs), in which the polarization of a ferroelectric material is reversed.[5,6] In the experiment, the thickness of the ferroelectric thin film can be as thin as several nanometers,[7–9] and the ferroelectric effect is preserved. It makes the ferroelectric tunnel junctions (FTJs) possible using nanoferroelectric films as tunnel barriers.[6,10,11] Compared to these three types of nonvolatile memories, RRAMs and FERAMs are only controlled by an electric field. The phase change in them requires some sort of atomic rearrangement that modulates the electronic current. MRAMs need one more degree, a magnetic field. The symmetry selection of spin current in barriers, such as MgO, modulates the spin current in the parallel and antiparallel magnetic configuration of two magnetic electrodes. The interfacial phases play a key role in all three types of nonvolatile memories because (1) the driving mechanism of RRAMs involves an interface-type conducting path, such as the electrochemical migration of oxygen vacancies[1,2]; (2) the interfacial electrode oxidation or oxygen vacancies in the barrier can strongly suppress the conductance in magnetic tunnel junctions[3,4]; (3) the electron transport in FTJs is very sensitive to the effect of an interface.[14–17] Besides the interfacial effect, the electrode,[11–13] impurity,[18–21] and strain[22–24] also play a key role in the electron transmission in FTJs. For example, the conductance of $BaTiO_3$ with Fe electrodes is five times that with Pt electrodes.[11,25] Wang *et al.* found that an intrinsically inactive conductance channel in $SrTiO_3$ opens after doping La or Nb for Sr or Ti, resulting in the enhancement of tunneling conductance.[18] Luo *et al.* proposed that the tunneling conductance of $PbTiO_3$ could be tuned by mechanical loads.[22] Therefore, a systematic study on the electron transport of FTJs under different environments, such as interface, oxidation and doping, is important for practical applications of ferroelectric tunnel junctions.

In this article, we systematically explore the ferroelectric, interfacial, oxidative, and doping effect on the tunneling conductance of the $Pt/BaTiO_3/Pt$ tunnel junction. Our results show that all these effects can affect the tunneling conductance of FTJs, but the physics behind them is different. The computational details of this work are given in Sec. II. We present details of the optimized structures in Sec. III. The results and discussions of four different effects on the tunneling conductance of the $Pt/BaTiO_3/Pt$ tunnel junction are given in Sec. IV and its subsections. The summary of this article is shown in Sec. V.

II. COMPUTATIONAL DETAILS

The first-principles density functional theory (DFT) calculation was performed by the pseudopotential plane-wave method[26] as implemented in the Vienna Ab-initio Simulation Package (VASP)[27,28] We adopted the generalized gradient approximation (GGA) proposed by Perdew *et al.*[29,30] for the exchange correlation energy functional. A plane-wave basis set was used to expand the Kohn-Sham orbitals with a 500-eV kinetic energy cutoff. We optimized the lattice parameters and atom positions using the conjugated-gradient algorithm based on Hellmann-Feynman forces. For the bulk Pt electrode optimization, we used a well converged $15 \times 15 \times 15$ Monkhorst-Pack grids for k-point sampling in the Brillouin zone of the fcc unitcell and the Hellmann-Feynman forces acting on each atom is less than 0.01 eV/Å in relaxed structures. For the relaxation of cubic $BaTiO_3$, a $4 \times 4 \times 4$ Monkhorst-Pack k-point in the Brillouin zone was used due

to the insulating property of $BaTiO_3$. The Hellmann-Feynman forces acting on each atom was the same as that of Pt electrodes ($\leqslant$0.01 eV/Å). The device optimization and quantum transport calculations were carried out within the framework of density functional theory combined with the nonequilibrium Green's function (NEGF) method as implemented in the ATOMISTIX TOOLKIT software package.[31,32] The GGA was adopted for the exchange and correlation functional and the double-ζ polarized basis set was used for the electron wave function of O, while the single-ζ polarized basis set was used for Pt, Ba, and Ti. Note that we also calculate the transmission using local-density approximations (LDA) and the calculated conductance is slightly larger than that using GGA, which does not affect our conclusions because their trend is the same. A cutoff energy of 150 Ry and a Monkhorst-Pack k-mesh of $6 \times 6 \times 100$ yielded a good balance between the computational time and accuracy in the results of the transport calculation, respectively. The NEGF-DFT self-consistency was controlled by a numerical tolerance of 10^{-5} eV. The electron temperature was set to 300 K in the transport calculation.

III. STRUCTURES

First, the structure of the bulk (fcc) Pt as electrodes is optimized. Its lattice constant is $a = b = c = 3.976$ Å [see Fig. 1(a)]. The calculated lattice constant of the cubic phase of $BaTiO_3$ is 4.033 Å [see Fig. 1(b)], which is larger than those of the LDA calculation (3.994 Å) (Ref. 33) and experimental value (3.991 Å) (Ref. 34). Next, we consider the junction structure of the device as a $BaTiO_3$ barrier sandwiched between two Pt electrodes. The in-plane lattice constant of the junction is fixed to be the experimental value of bulk $BaTiO_3$ of 3.991 Å, which is smaller than the above calculated lattice constant of $BaTiO_3$, but larger than the calculated lattice constant of Pt. Thus, it produces a tetragonal distortion of both $BaTiO_3$ and Pt. To calculate the distortion, we fix the volume of the calculated unitcell of $BaTiO_3$ and Pt and the in-plane lattice constant ($a = b = 3.991$ Å). The calculated c of Pt and $BaTiO_3$ are 3.946 Å and 4.118 Å, respectively. Correspondingly, the tetragonal distortion (c/a) is 0.99 and 1.03 for Pt and $BaTiO_3$, respectively [see Figs. 1(c) and 1(d)].

Since there are two surfaces of $BaTiO_3$, BaO, and TiO_2 termination, we examine different interfacial structures to seek the most energetically stable one. Both BaO- and TiO_2-terminated surfaces are considered. Each of them has two contacting sites with the outmost layer of Pt electrodes [see Figs. 1(e) and 1(f)]. One is that the O atoms or Ti atoms in TiO_2 termination are located on the top of the outmost Pt layer [see Fig. 1(e)]. The other is that the Ba/O atoms or the hollow site in BaO termination are located on the top of the outmost Pt layer [see Fig. 1(f)]. Thus, there are four different interfacial structures [see Table I]. For the electronic structure calculations of the $Pt/BaTiO_3$ system, the most stable interface structure is found by comparing the interfacial energies of Pt on the $BaTiO_3$ surface. The interfacial energy is defined by:[35,36]

$$E_{\text{int}} = \left(E_{\text{Pt}} + E_{\text{BaTiO}_3} - E_{\text{Pt/BaTiO}_3}\right)/A, \tag{1}$$

where $E_{\text{Pt/BaTiO}_3}$ is the energy of the supercell of the $Pt/BaTiO_3$ interfacial structure. E_{Pt} and E_{BaTiO_3} are the corresponding energies of the Pt or $BaTiO_3$ single component slab. A is the interface area. The calculated values of the interfacial energies

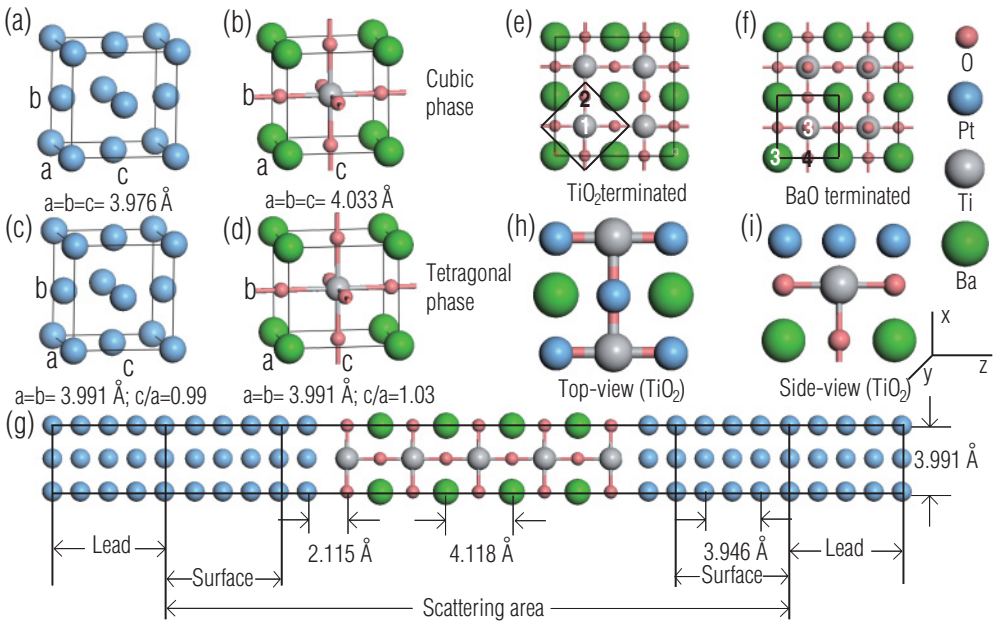

FIG. 1. (Color online) Structural optimization of the $Pt/BaTiO_3$ ferroelectric tunneling junction. (a) and (b) are the cubic phase of Pt electrodes and the $BaTiO_3$ barrier. The in-plane lattice constants a and b are fixed by the experimental values of $BaTiO_3$ of 3.991 Å, resulting in the tetragonal phase of (c) Pt electrodes and (d) the $BaTiO_3$ barrier with the c/a value of 0.99 and 1.03, respectively. (e) and (f) are the interfacial structures of TiO_2-terminated and BaO-terminated $Pt/BaTiO_3$ with different contacted sites by the Pt atoms. The Pt atoms sit on the top of Ti atoms (1 site) or O atoms (2 site). The Pt atoms site on the top of Ba and O atoms (3 site) or the hollow sites (4 site). Top (h) and side (i) views of the most favorite interface structure (2 site) with the interfacial distance of 2.115 Å. The model of the $Pt/BaTiO_3$ junction with the optimized lattice constant, interfacial structure, and interfacial distance is shown in (g).

TABLE I. Calculated interfacial energies E_{int} (eV/nm^2), and the interfacial distance d_{int} (Å) for different Pt/$BaTiO_3$ interfaces shown in Figs. 1(e) and 1(f).

Interface	Site	E_{int}	d_{int}
TiO_2	1[a]	7.11	3.112
	2[b]	27.02	2.115
BaO	3[c]	24.40	3.061
	4[d]	20.21	2.233

[a]Fig. 1(e).
[b]Fig. 1(e).
[c]Fig. 1(f).
[d]Fig. 1(f).

for the four cases are shown in Table I. It shows that the most stable interfacial structure of Pt/$BaTiO_3$ is that the O atoms sit on the top of the outmost Pt atoms in the TiO_2-terminated surface [see Figs. 1(h) and 1(i)]. This is the reason why most previous works considered only the TiO_2-termination case.[11,18,22]

At the end, we calculate the distance between Pt electrodes and the $BaTiO_3$ barrier (i.e., the interfacial distance of the Pt/$BaTiO_3$/Pt junction). We fix the in-plane lattice constant (3.991 Å) and use the optimized lattice constant of c of both Pt and $BaTiO_3$. Both surfaces of $BaTiO_3$ at the two interfaces are TiO_2 terminated based on our calculated adsorption energies in Table I. We relax the whole structure until the stress is less than 0.005 eV/Å^3. The optimized interfacial distance is 2.115 Å. Based on the above structural calculations, we calculate the lattice constant of Pt electrodes and the $BaTiO_3$ barrier, the interfacial type, and interfacial distance. Thus, we can get the final optimized structure of the Pt/$BaTiO_3$/Pt tunnel junction, which is shown in Fig. 1(g).

IV. RESULTS AND DISCUSSIONS

A. Ferroelectric effect

The most important property of $BaTiO_3$ is its ferroelectric effect.[10,11,37,38] Under the external electric field, there is an electric polarization in $BaTiO_3$ resulting in the atomistic distortion of Ti and O atoms. In this section, we investigate the ferroelectric effect on the electron transport, especially the tunneling conductance in the Pt/$BaTiO_3$/Pt tunnel junction. The $BaTiO_3$ barrier is composed of five layers of TiO_2 and four layers of BaO, which is sandwiched between two semi-infinite Pt electrodes. Two interfaces, between the Pt electrode and $BaTiO_3$ barrier, are both Pt-TiO_2 with interfacial distance of 2.115 Å. We consider two structures. One is the nonferroelectric (NFE) structure,[39] in which the in-plane (xy plane) atoms are frozen artificially. The relaxed structure of NFE is shown in Fig. 2(a). The other is the ferroelectric structure,[11] in which all positions are completely relaxed until the force and stress are less than 0.01 eV/Åand 0.005 eV/Å^3, respectively. The displacement of Ti-O, after optimization, results in a stable ferroelectric ground state. The relaxed displacement of Ti-O, δ, with respect to the planar Ti-O positions in the FE structure are shown in Fig. 2(b). The arrows in Fig. 2(b) show displacements of Ti atoms with respect to O atoms within each TiO_2 layer. As can be seen, the displacement is asymmetry at two interfaces, which is in good agreement with the other calculations of Pt/$BaTiO_3$/Pt (Ref. 11) or Fe/$BaTiO_3$/Fe (Ref. 37). This asymmetry behavior is due to the dissimilar electrostatic potentials, induced by the electrodes, at the two interfaces. The local density of state (DOS) of two Ti-3d states at two interfaces shows a rigid shift of about 0.2 eV, which reflects the asymmetry of displacements at two interfaces.[11] Moreover, the displacement in the central TiO_2 is only 0.05 Å which is smaller than the experimental values of bulk $BaTiO_3$ (0.12∼0.23 Å) due to the effect of the electrodes.

The tunneling conductance of NFE (G_{NFE}) and FE (G_{FE}) are calculated using the DFT and NEGF methods. The calculated G_{NFE} and G_{FE} are $2.339 \times 10^{-3}\ G_0$ and $4.217 \times 10^{-4} G_0$, respectively (Table II), where $G_0 = 2e^2/h$, e and h are the electron charge and Planck's constant, respectively. It implies that ferroelectric displacements produce a significant change in tunneling conductance. The three-dimensional (3D) $\mathbf{k}_{\parallel}$-resolved transmission is shown in Fig. 3. As can be seen, the main contribution to the tunneling conductance in the

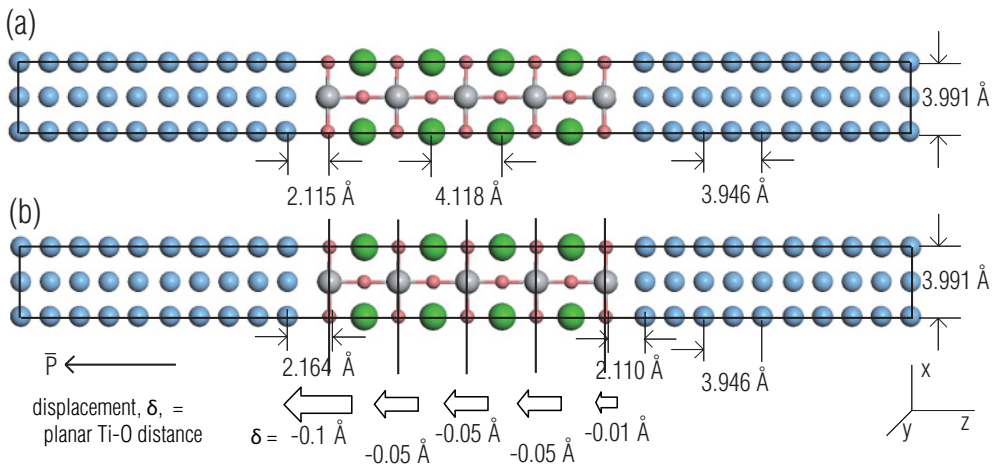

FIG. 2. (Color online) Optimized structures of the Pt/$BaTiO_3$ tunneling junction. The electric polarization direction is $-z$. Arrows show displacements of the Ti atoms with respect to O atoms within each planar TiO_2 layer for (a) nonferroelectric (NFE) and (b) ferroelectric (FE) ground states of $BaTiO_3$. The displacement at two interfaces is different due to the effect of electrodes.

TABLE II. Calculated tunneling conductance (G_0) for different $Pt/BaTiO_3/Pt$ structures

Interface	Ground state	Tunneling conductance
TiO_2	NFE	2.339×10^{-3}
	FE	4.217×10^{-4}
BaO	FE	1.308×10^{-5}
O rich	FE	8.686×10^{-8}
O poor	FE	1.482×10^{-4}
Nb doping	FE	1.558×10^{-1}

$Pt/BaTiO_3/Pt$ tunnel junction comes from the region around the Brillouin zone center (i.e., Γ point). We note that the profile of the $\mathbf{k}_\parallel$-resolved transmission is similar to that of the $\mathbf{k}_\parallel$-resolved DOS at the Fermi energy,[11] which indicates the electron transport at the Fermi energy in the $Pt/BaTiO_3/Pt$ tunnel junction is dominated by resonant tunneling through interface states of Bloch states with wave vectors near the Γ point. Therefore, the symmetry interfacial structure in the NFE state is the main reason that the tunneling conductance of the NFE state is higher than that of the FE state, in which the interface states are asymmetric [see Fig. 1(b)]. In other words, the large barrier width, induced by the large interfacial distance (2.164 Å), is not the main reason for the small tunneling conductance in the NFE state.

To understand the physics of transport decay due to the ferroelectric effect, the complex band structure of the $Pt/BaTiO_3/Pt$ tunnel junction is studied since a wave function can be described in terms of irreducible representations of the crystal's symmetry group.[40] For example, in Fe/MgO/Fe MTJs, the electrodes, Fe, and the insulating barrier, MgO, are the cubic space group, in which the Δ_1 band composes of p_z and d_{z^2} orbitals, while the Δ_5 band composes of p_x, p_y d_{xz}, and d_{yz} orbitals and the Δ_2 band is composed of $d_{x^2-y^2}$. If the electrodes and insulating barrier have the same band symmetry, their Bloch states are coupled to a given evanescent state and sustain a tunneling current with a small decay.[40,41] This is the so-called "symmetry selective filter." For example, the Fe majority carrier Δ_1 band couples efficiently with the Δ_1 complex band in MgO, while its minority carriers can only couple through the Δ_5 and Δ_2 bands, which decay much faster. Recently, Stewart theoretically argued that a C_{2v} oxide, $Mg_3B_2O_6$, could also show good tunneling with the FeCo electrodes of the C_{4v} space group.[42]

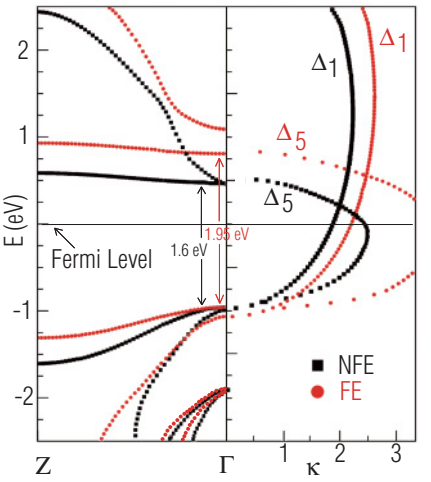

FIG. 4. (Color online) The real and complex band structures for $BaTiO_3$ in NFE and FE states. The Fermi level is set to zero by a solid line. The wave-function symmetries of the bands close to the Fermi level, Δ_1 and Δ_5, are indicated.

Figure 4 shows the real and complex band structure of the ferroelectric $BaTiO_3$, which is in good agreement with other calculations.[11,39] As can be seen, the complex band structure of BTO is similar to that of $SrTiO_3$ with two evanescent states of Δ_1 and Δ_5 bands, which have the lowest decay rates.[11] But the complex band structure of BTO is slightly different from that of MgO, where states with the Δ_5 band decay significantly faster than those with the Δ_1 band.[40,41] In $BaTiO_3$, the Δ_1 band has a similar decay rate both in NFE and FE. However, the ferroelectric effect enhances the band gap resulting in a large decay rate of the Δ_5 band compared to the nonferroelectric state. This enhancement of the decay rates of the Δ_5 band explains the conductance drop by ferroelectric effects.

B. Interfacial effect

From the calculated adsorption energy of the Pt/BTO interface system in Table I, the most stable interfacial structure

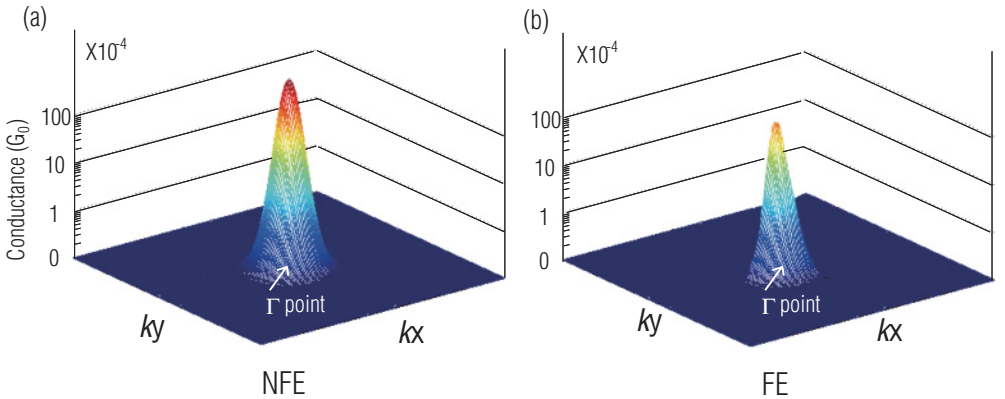

FIG. 3. (Color online) 3D k-resolved tunneling conductance at the Fermi level for the (a) NFE and (b) FE states of the $Pt/BaTiO_3$ tunneling junction.

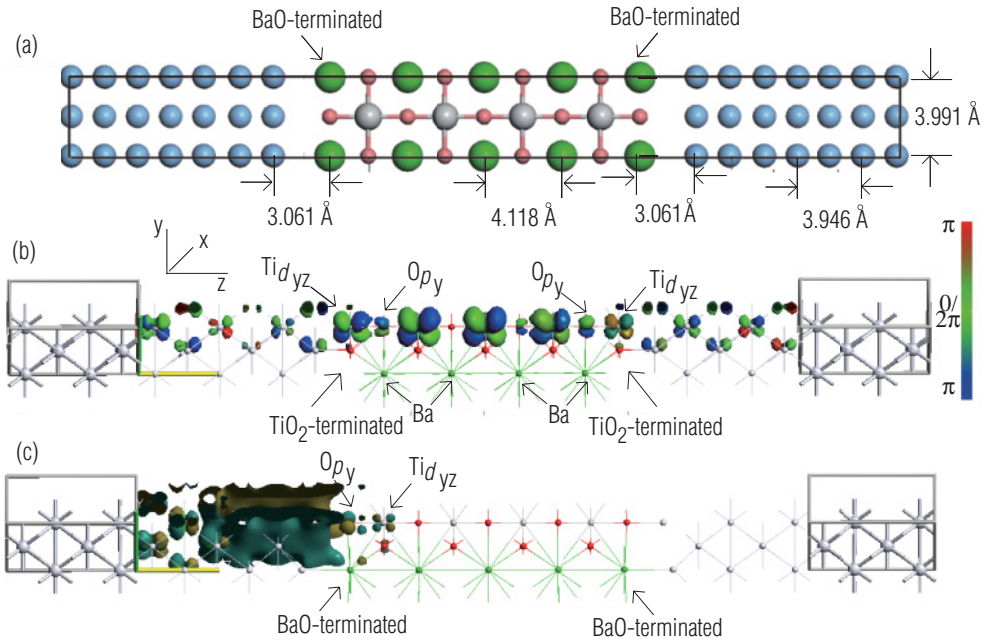

FIG. 5. (Color online) (a) The optimized structure of the Pt/BaO-BTO-BaO/Pt tunneling junction. (b) The transmission eigenstate of the structure of Pt/TiO_2-BTO-TiO_2/Pt. (c) The transmission eigenstate of the structure of Pt/BaO-BTO-BaO/Pt. There is a decay of the transmission eigenstate from the left interface to the right interface due to scattering by the BaO layer at the interface. The d_{yz} orbital of Ti and the p_y orbital of O contribute to the electron transfer channel, while the orbitals of Ba have few contributions.

is the TiO_2-terminated surface contacted with the Pt electrode, in which the Pt atoms sit on the top sites of the oxygen atoms of TiO_2-terminated surface. Moreover, the interfacial energy of Pt on the TiO_2 terminated surface (2 site in Fig. 1(e)) is more energetically favored than on the BaO-terminated surface (3 site in Fig. 1(f)) with the interfacial energy difference of 2.62 eV/nm^2. However, the calculated energy difference between the TiO_2 termination and BaO termination is not large enough to overcome the thermal effect under a high annealing temperature. It is quite possible to form the Pt-BaO interface during the fabrication of Pt/BTO/Pt MTJs in the experiment. Therefore, we consider the interfacial effect, either Pt-TiO_2 or Pt-BaO, on the tunneling conductance for the Pt/BTO/Pt junction.

Figure 5(a) shows the optimized structure of Pt/BaO-BTO-BaO/Pt. The $BaTiO_3$ barrier has the same ferroelectric ground state as that in Pt/TiO_2-BTO-TiO_2/Pt with two Pt-TiO_2 interfaces. The calculated tunneling conductance of Pt/BaO-BTO-BaO/Pt is $1.308 \times 10^{-5}\ G_0$, which is one order of magnitude lower than that of Pt/TiO_2-BTO-TiO_2/Pt [see Table I]. To understand the low tunneling conductance induced by the BaO-terminated interface, we calculated the 3D isovalue of the transmission eigenstate, which is shown in Figs. 5(b) and 5(c). The electron transmission eigenstate shows that electrons mainly flow through Ti-O bonding states, while few electrons flow through the Ba-O bond. Within the tunneling barrier, the volume of isovalues of the transmission eigenstate dramatically decays from the high bias termination to the low bias termination (left to right). We note that no transmission eigenstate is around the left BaO-terminated interface due to the strong scattering to electrons, resulting in the same poor tunneling conductance as that of Pt/TiO_2-BTO-TiO_2/Pt. Moreover, we can see that the electron transport channel, Ti-O bonding states, is composed by O-p_y orbitals (Δ_1 band) and Ti-d_{yz} orbitals (Δ_5 band). These two bands have much smaller decay rates in the complex band structure of $BaTiO_3$ [see Fig. 4]. Therefore, a direct figure of the electron transport can be given by the transmission eigenstate as well as the complex band structure.

C. Oxidative effect

To fabricate the ferroelectric tunnel junctions experimentally one needs to grow the oxide surface first and then deposit the metal electrodes.[43–45] It is inevitable to form either the overoxidization or underoxidization under oxygen-rich or oxygen-poor conditions. Therefore, the effect of interfacial oxidation on the tunneling conductance is very important to the tunneling junctions.[46] Here, we investigate the overoxidative (O rich) and underoxidative (O poor) interfacial effect on the tunneling conductance of the Pt/BTO/Pt system. The optimized structures of overoxidative and underoxidative interfacial Pt/BTO/Pt junctions are shown in Fig. 6. In the overoxidative interface, the Ti atoms at the TiO_2-terminated surface are replaced by O atoms. In the underoxidative interface, the O atoms at the TiO_2-terminated surface are replaced by Ti atoms, not leaving a O vacancy. This is because it is hard to form the O vacancy defect in tunneling junctions after a high temperature annealing. The calculated tunneling conductances of overoxidative and underoxidative interfaces are shown in Table II. As can be seen, there is a very strong suppression of the tunneling current in the O-rich interface ($8.686 \times 10^{-8} G_0$). There are two factors resulting in the poor conductance. One is that the interfacial oxygen acts likes an electron trap, which can trap electrons.[47] The other is that the Pt-d orbitals do not

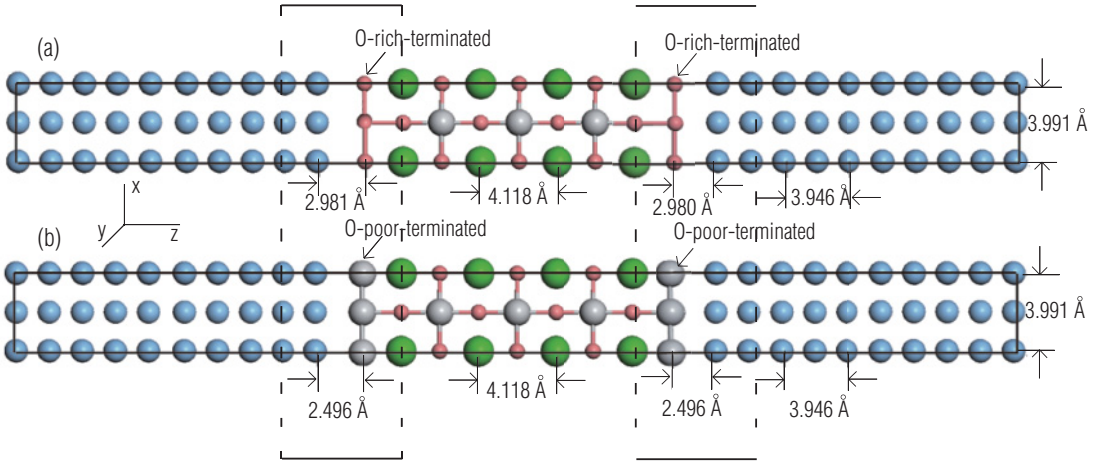

FIG. 6. (Color online) The optimized structures of the $Pt/BaTiO_3/Pt$ tunneling junction with the (a) O-rich and (b) O-poor interfaces.

mix with the O-p orbitals due to the local charge redistribution induced by additional oxygen atoms, which is also the reason for the much reduced magnetic anisotropy and the tunneling magnetoresistance (TMR) in Fe/MgO/Fe junctions with the overoxidative interface.[3,46] Since the hybridization of the Pt-d and O-p orbitals is preserved in the underoxidative interface, the conductance value ($1.482 \times 10^{-4} G_0$) is much higher than that of the overoxidative case but lower than that of the ideal, pure, Pt-TiO_2 interface ($4.217 \times 10^{-4} G_0$). This is similar to the case of Fe/MgO/Fe MTJs, in which the TMR is strongly suppressed by the interfacial oxidation while it can be recovered if a metal layer [such as Co (Ref. 48) and V (Ref. 49)] is inserted into the interface.

D. Doping effect

Experimentally, to modify the electronic structure of $BaTiO_3$ and to tailor its electronic properties, doping is the

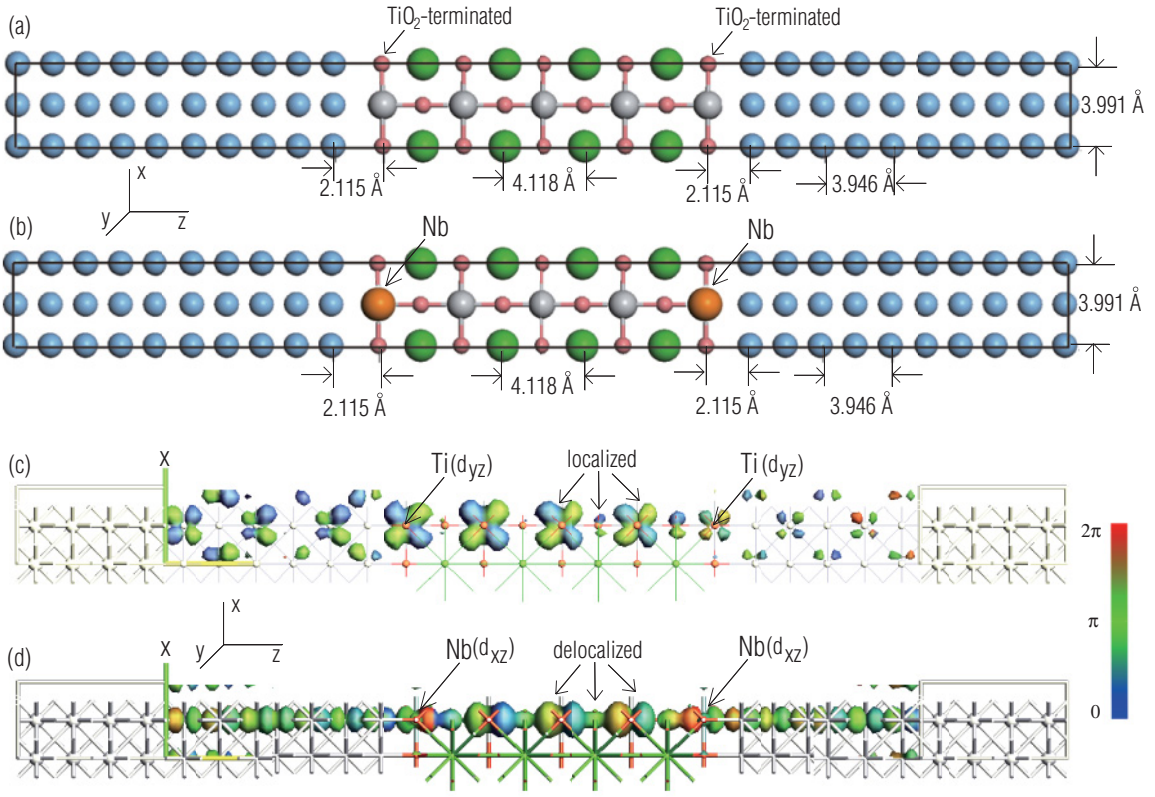

FIG. 7. (Color online) The optimized structures of the $Pt/BaTiO_3/Pt$ tunneling junctions (a) without and (b) with Nb doping. (c) and (d) the transmission eigenstates of undoped and doped $Pt/BaTiO_3/Pt$ tunneling junctions. The delocalized states of central Ti and O atoms opens the transmission channel, resulting in a good conductance.

most popular method.[19–21] Doping can change the initially insulating $BaTiO_3$ into a semiconducting or metallic state by the substitution of a pentavalent rare-earth ion, such as Nb, on quadrivalent Ti. Based on the calculated transmission eigenstates of $BaTiO_3$ in Fig. 5(b), we know that only one species of conductance channels comprised of the corner-shared TiO_6 octahedra (i.e., Ti-O bonding states in $BaTiO_3$). It is generally believed that the enhanced electron conductance in $BaTiO_3$ by Nb doping is due to the introduction of electrons. These introduced electrons reduce the amount of Ti^{4+} to Ti^{3+}, resulting in the electron transfer between Ti ions mediated by O (Ref. 18). First-principles calculations show that the Fermi level in Nb-doped ABO_3 systems is pushed up to the conduction band.[50] Therefore, we believe that Nb doping can affect the electron transport properties of $Pt/BaTiO_3/Pt$ junctions. The structure of Nb-doped $BaTiO_3$ is shown in Fig. 7(b). The interfacial Ti ions of the $Pt/BaTiO_3$ junction are substituted by the same Nb ions as that in the experiment.[19–21] The ground state of BTO is ferroelectric in our calculations.

Figures 7(c) and 7(d) show the transmission eigenstates for the optimized Pt/BTO/Pt junctions without and with Nb doping. The transmission eigenstates indicate the electron wave function along the conductance channel. As can be seen, the electron charges on the central Ti and O ions are localized in the undoped Pt/BTO/Pt junction, resulting in the closed electron transport channel. It can be explained for the insulating nature of pristine $BaTiO_3$ and the tunneling transport in the Pt/BTO/Pt junction. In the undoped Pt/BTO/Pt system, the overall features of transmission eigenstates at two interfaces are similar due to the symmetric structure. After doping by Nb, a main difference compared to the undoped case is that the electron charges become delocalized and are along the whole conductance channel. Especially, the electron charges on the Ti and O ions are delocalized and overlapped. The opening of the electron transport channel results in a large conductance of $1.558 \times 10^{-1} G_0$. It is about three orders of magnitude higher than the undoped case [see Table II]. Moreover, the electron charges are accumulated at the two interfacial areas due to the gap states induced by the two electrodes.[11,18] The tails of Pt metallic states penetrate into the insulating barrier.

V. CONCLUSION

In summary, the tunneling conductance of the $Pt/BaTiO_3/Pt$ tunnel junction is sensitive to the ferroelectric, interfacial, oxidative, and doping effects. The physics mechanism behind these phenomena is investigated by the transmission eigenstates. Our systematical studies of the tunneling transmission pave a way to the practical applications of ferroelectric tunneling junctions and other ferroelectric devices.

ACKNOWLEDGMENTS

The authors thank the helpful discussion of Yang Ming and Lu Yunhao. This work is partially supported by A*STAR (Singapore) Research Founding (Grants No. 092-156-0120, No. 092-156-0121, and No. DSI/10-100012).

*Present address: Department of Physics, National University of Singapore.
†phyfyp@nus.edu.sg

[1] A. Sawa, Mater. Today **11**, 28 (2008).
[2] D. B. Strukov, G. S. Snider, D. R. Stewart, and R. S. Williams, Nature (London) **453**, 80 (2008).
[3] Y. Ke, K. Xia, and H. Guo, Phys. Rev. Lett. **100**, 166805 (2008).
[4] Y. Ke, K. Xia, and H. Guo, Phys. Rev. Lett. **105**, 236801 (2010).
[5] M. Dawber, K. M. Rabe, and J. F. Scott, Rev. Mod. Phys. **77**, 1083 (2005).
[6] E. Y. Tsymbal and H. Kohlstedt, Science **313**, 181 (2006).
[7] D. Fong, G. Stephenson, S. Streiffer, J. Eastman, O. Auciello, P. Fuoss, and C. Thompson, Science **304**, 1650 (2004).
[8] D. A. Tenne, A. Bruchhausen, N. D. Lanzillotti-Kimura, A. Fainstein, R. S. Katiyar, A. Cantarero, A. Soukiassian, V. Vaithyanathan, J. H. Haeni, W. Tian, D. G. Schlom, K. J. Choi, D. M. Kim, C. B. Eom, H. P. Sun, X. Q. Pan, Y. L. Li, L. Q. Chen, Q. X. Jia, S. M. Nakhmanson, K. M. Rabe, and X. X. Xi, Science **313**, 1614 (2006).
[9] C. Lichtensteiger, J. M. Triscone, J. Junquera, and P. Ghosez, Phys. Rev. Lett. **94**, 047603 (2005).
[10] G. Gerra, A. K. Tagantsev, N. Setter, and K. Parlinski, Phys. Rev. Lett. **96**, 107603 (2006).
[11] J. P. Velev, C. G. Duan, K. D. Belashchenko, S. S. Jaswal, and E. Y. Tsymbal, Phys. Rev. Lett. **98**, 137201 (2007).
[12] M.-Q. Cai, Y. Zheng, P.-W. Ma, and C. H. Woo, J. Appl. Phys. **109**, 024103 (2011).
[13] J. P. Velev, C. G. Duan, J. D. Burton, A. Smogunov, M. K. Niranjan, E. Tosatti, S. S. Jaswal, and E. Y. Tsymbal, Nano Lett. **9**, 427 (2009).
[14] E. Y. Tsymbal, K. D. Belashchenko, J. P. Velev, S. S. Jaswal, M. van Schilfgaarde, I. I. Oleynik, and D. A. Stewart, Prog. Mater. Sci. **52**, 401 (2007).
[15] H. Choi, Y. Hwang, E.-K. Lee, and Y.-C. Chung, J. Appl. Phys. **109**, 07D909 (2011).
[16] X. Feng, O. Bengone, M. Alouani, S. Lebegue, I. Rungger, and S. Sanvito, Phys. Rev. B **79**, 174414 (2009).
[17] M. K. Niranjan, J. D. Burton, J. P. Velev, S. S. Jaswal, and E. Y. Tsymbal, Appl. Phys. Lett. **95**, 052501 (2009).
[18] Z. Wang, S. Tsukimoto, M. Saito, and Y. Ikuhara, Appl. Phys. Lett. **94**, 252103 (2009).
[19] D. Nagano, H. Funakubo, K. Shinozaki, and N. Mizutani, Appl. Phys. Lett. **72**, 2017 (1998).
[20] E. Patino, F. Erazo, and A. Stashans, Mater. Lett. **50**, 337 (2001).
[21] E. Patino and A. Stashans, Ferroelectrics **256**, 189 (2001).
[22] X. Luo, B. Wang, and Y. Zheng, ACS Nano **5**, 1649 (2011).
[23] J. H. Lee and K. M. Rabe, Phys. Rev. Lett. **107**, 067601 (2011).
[24] J. H. Lee and K. M. Rabe, Phys. Rev. Lett. **104**, 207204 (2010).
[25] J. P. Velev, C.-G. Duan, K. D. Belashchenko, S. S. Jaswal, and E. Y. Tsymbal, J. Appl. Phys. **103**, 07A701 (2008).

[26]G. Kresse and J. Furthmuller, Comput. Mater. Sci. **6**, 15 (1996); **54**, 11169 (1996).
[27]G. Kresse and J. Hafner, Phys. Rev. B **47**, 558 (1993); **49**, 14251 (1994).
[28]G. Kresse and D. Joubert, Phys. Rev. B **59**, 1758 (1999).
[29]J. P. Perdew and Y. Wang, Phys. Rev. B **45**, 13244 (1992).
[30]J. P. Perdew, K. Burke, and M. Ernzerhof, Phys. Rev. Lett. **77**, 3865 (1996).
[31]J. Taylor, H. Guo, and J. Wang, Phys. Rev. B **63**, 121104 (2001).
[32]J. Kurti, C. Magyar, A. Balazs, and P. Rajczy, Synthetic. Met. **71**, 1865 (1995).
[33]Ph. Ghosez, X. Gonze, and J.-P. Michenaud, Ferroelect. **220**, 1 (1999).
[34]G. H. Kwei, A. C. Lawson, S. J. L. Billinge, and S. W. Cheong, J. Phys. Chem. **97**, 2368 (1993).
[35]I. I. Oleinik, E. Y. Tsymbal, and D. G. Pettifor, Phys. Rev. B **62**, 3952 (2000).
[36]I. I. Oleinik, E. Y. Tsymbal, and D. G. Pettifor, Phys. Rev. B **65**, 020401 (2001).
[37]C. G. Duan, S. S. Jaswal, and E. Y. Tsymbal, Phys. Rev. Lett. **97**, 047201 (2006).
[38]P. Aguado-Puente and J. Junquera, Phys. Rev. Lett. **100**, 177601 (2008).
[39]N. M. Caffrey, T. Archer, I. Rungger, and S. Sanvito, Phys. Rev. B **83**, 125409 (2011).
[40]W. H. Butler, X. G. Zhang, T. C. Schulthess, and J. M. MacLaren, Phys. Rev. B **63**, 054416 (2001).
[41]X. G. Zhang and W. H. Butler, Phys. Rev. B **70**, 172407 (2004).
[42]D. A. Stewart, Nano Lett. **10**, 263 (2010).
[43]V. Garcia, S. Fusil, K. Bouzehouane, S. Enouz-Vedrenne, N. D. Mathur, A. Barthelemy, and M. Bibes, Nature (London) **460**, 81 (2009).
[44]V. Garcia, M. Bibes, L. Bocher, S. Valencia, F. Kronast, A. Crassous, X. Moya, S. Enouz-Vedrenne, A. Gloter, D. Imhoff, C. Deranlot, N. D. Mathur, S. Fusil, K. Bouzehouane, and A. Barthelemy, Science **327**, 1106 (2010).
[45]P. Maksymovych, S. Jesse, P. Yu, R. Ramesh, A. P. Baddorf, and S. V. Kalinin, Science **324**, 1421 (2009).
[46]X. G. Zhang, W. H. Butler, and A. Bandyopadhyay, Phys. Rev. B **68**, 092402 (2003).
[47]L. Shen, M. Zeng, S.-W. Yang, C. Zhang, X. Wang, and Y. Feng, J. Am. Chem. Soc. **132**, 11481 (2010).
[48]Y. Wang, X. F. Han, and X.-G. Zhang, Appl. Phys. Lett. **93**, 172501 (2008).
[49]X. Feng, O. Bengone, M. Alouani, I. Rungger, and S. Sanvito, Phys. Rev. B **79**, 214432 (2009).
[50]N. Shanthi and D. D. Sarma, Phys. Rev. B **57**, 2153 (1998).